Crystal structure and partial Ising-like magnetic ordering of orthorhombic Dy_2TiO_5

Jacob Shamblin,[1,2] Stuart Calder,[3] Zhiling Dun,[2] Minseong Lee,[4,5] Eun Sang Choi,[4] Joerg Neuefeind,[6] Haidong Zhou,[2,*] and Maik Lang[1,†]

[1]*Department of Nuclear Engineering, University of Tennessee, Knoxville, Tennessee 37996, USA*
[2]*Department of Physics and Astronomy, University of Tennessee, Knoxville, Tennessee 37996, USA*
[3]*Oak Ridge National Laboratory, Quantum Condensed Matter Division, Oak Ridge, Tennessee 37831, USA*
[4]*Florida State University, Department of Physics, Tallahassee, Florida 32306, USA*
[5]*Florida State University, National High Magnet Field Laboratory, Tallahassee, Florida 32310, USA*
[6]*Chemical and Engineering Materials Division, Spallation Neutron Source, Oak Ridge National Laboratory, Oak Ridge, Tennessee 37831, USA*

(Received 18 March 2016; published 12 July 2016)

The structure and magnetic properties of orthorhombic Dy_2TiO_5 have been investigated using x-ray diffraction, neutron diffraction, and alternating current (ac)/direct current (dc) magnetic susceptibility measurements. We report a continuous structural distortion below 100 K characterized by negative thermal expansion in the [0 1 0] direction. Neutron diffraction and magnetic susceptibility measurements revealed that two-dimensional (2D) magnetic ordering begins at 3.1 K, which is followed by a three-dimensional magnetic transition at 1.7 K. The magnetic structure has been solved through a representational analysis approach and can be indexed with the propagation vector $k = [0\ 1/2\ 0]$. The spin structure corresponds to a coplanar model of interwoven 2D "sheets" extending in the [0 1 0] direction. The local crystal field is different for each Dy^{3+} ion (Dy1 and Dy2), one of which possesses strong uniaxial symmetry indicative of Ising-like magnetic ordering. Consequently, two succeeding transitions under magnetic field are observed in the ac susceptibility, which are associated with flipping each Dy^{3+} spin independently.

DOI: 10.1103/PhysRevB.94.024413

I. INTRODUCTION

Insulators of general formula A_2TiO_5 have attracted significant attention in recent years due to their structural and chemical diversity. Depending on the A-site cation size and/or sample synthesis method, these complex oxides can form cubic, orthorhombic, hexagonal, and monoclinic polymorphs without altering the stoichiometry [1–5]. As a result, these materials are suitable for a wide array of technological applications, including potential actinide hosts for long-term storage in a geological repository [6–8], ion conductors for fuel cells and oxygen sensors [2], and nanoparticles in oxide dispersion strengthened (ODS) steels [9]. These materials can readily incorporate rare-earth elements into their A site, resulting in many complex magnetic interactions. They are frequently end members in solid solution series of general formula $Ln_2(Ti_{2-x}Ln_x)O_{7-x/2}$ (often referred to as "stuffed pyrochlores"), in which magnetic lanthanide elements are incrementally stuffed into the $Ln_2Ti_2O_7$ pyrochlore matrix, increasing the relative number of spins involved in magnetic interactions [10]. $Ho_2Ti_2O_7$, for example, forms the well-studied spin-ice state at low temperatures with locally ordered magnetic moments analogous with protons in water ice [11,12]. Stuffing additional magnetic Ho^{3+} atoms into the pyrochlore causes interesting, and seemingly counterintuitive, behavior [13]. A fully stuffed $Ho_2(Ti_{2-x}Ho_x)O_{7-x/2}$ corresponds to $Ho_{2.67}Ti_{1.33}O_{6.67}(x = 0.67)$ or Ho_2TiO_5. Depending on the sample synthesis method, this disorders the pyrochlore (at least partially) into the isometric defect-fluorite average structure with cation mixing between Ho^{3+} and Ti^{4+} crystallographic sites. The structure is effectively converted from a network of corner-sharing tetrahedra, essential for the spin-ice state, to a network of side-sharing tetrahedra with intrinsic disorder. Despite the increased concentration of magnetic moments and partially disordered structure, the zero-point entropy per spin characteristic of frustration remains more or less unchanged from that of the original pyrochlore spin ice [13]. Other stuffed pyrochlores with cubic Ln_2TiO_5 end members have also been studied in detail for both structural and magnetic properties [10]. Interestingly, none of these displayed evidence of long-range magnetic order above 2 K. Magnetic interactions were shown to be predominately antiferromagnetic, while Ln^{3+} spins were shown to be strongly anisotropic, similar to spin ice.

However, magnetic properties of the orthorhombic polymorphs have not been fully characterized. For example, $Dy_2Ti_2O_7$ is another prototypical spin ice [14] that can be readily transformed into an orthorhombic polymorph through the stuffing procedure [3]. The fully stuffed Dy_2TiO_5 end member (*Pnma* space group) is an important material in the nuclear power industry, where due to dysprosium's large thermal neutron absorption cross section ($\sigma_a = 997$ b), it is used as a neutron absorber in control rods in Russian Voda Voda Energo Reactor (VVER)-type reactors [15,16]. This, however, makes Dy-based compounds difficult to characterize with neutron diffraction, which has perhaps deterred detailed studies into any magnetic structure. Dy_2TiO_5 is isostructural, with orthorhombic Y_2TiO_5 first reported by Mumme [1], in which Y^{3+} (or Dy^{3+}, in this case) and Ti^{4+} are 7- and 5-coordinated with oxygen, respectively [Fig. 1(a)]. This mixture of seven- and fivefold coordination is rather unique compared with other rare earth titanates

*Corresponding authors: HZhou10@utk.edu
†MLang2@utk.edu

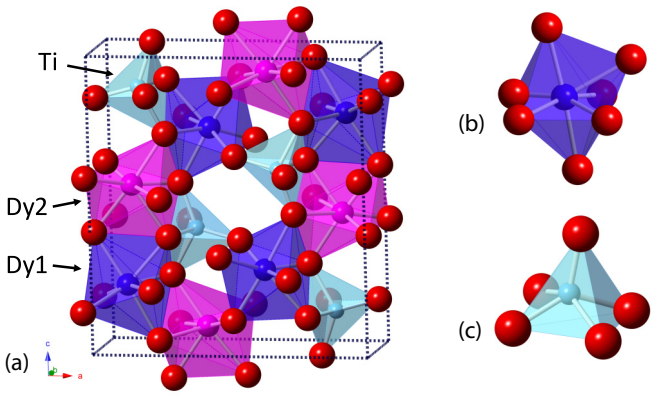

FIG. 1. (a) Structure of orthorhombic Dy_2TiO_5 (*Pnma* space group). (b) Dy atoms are in monocapped octahedral coordination (shown as blue and magenta polyhedra for Dy1 and Dy2, respectively). (c) Ti atoms are in square pyramidal coordination.

of the same ternary system (such as pyrochlore or layered perovskites), in which Ln^{3+} and Ti^{4+} usually form distorted cubes and octahedra, respectively. Here, the 7-coordinated Ln^{3+} ions are in a monocapped octahedral configuration, while the five-coordinated Ti^{4+} ions form square pyramidal polyhedra [Figs. 1(b) and 1(c)]. All atoms are located in distinct 4*c* Wyckoff positions, each of which requiring an x and z coordinate to describe the atomic positions within the unit cell. This creates structural flexibility, allowing for significant distortions of local polyhedra. While both Dy^{3+} ions form similar monocapped octahedra locally, they are coordinated differently at longer scales. The first Dy^{3+} monocapped octahedron, from now on referred to as Dy1, is edge sharing with five additional monocapped octahedra and two square pyramids and is corner sharing with the apex of two square pyramids and the basal corner of one square pyramid. The second Dy^{3+} octahedron, Dy2, is edge sharing with seven monocapped octahedra and two square pyramids and is corner sharing with the basal corner of one square pyramid. The magnetic properties of this orthorhombic polymorph of Dy_2TiO_5 remains unexplored to this point. One consequence of the differing connectivity for each Dy^{3+} ion creates is the distinct possibility of magnetic moments that can order independently for both Dy1 and Dy2. In this paper, we investigate the low temperature crystal structure and magnetic order of orthorhombic Dy_2TiO_5 using a combination of x-ray diffraction (XRD), neutron diffraction, and alternating current (ac)/direct current (dc) magnetic susceptibility measurements.

II. EXPERIMENT

A. Sample synthesis

Stoichiometric mixtures of Dy_2O_3 and TiO_2 were combined in the following solid-state reaction:

$$Dy_2O_3 + TiO_2 \rightarrow Dy_2TiO_5$$

Dy_2O_3 was prefired at 1000 °C for 8 h to remove any adsorbed water. Powders were ground, mixed using an acetone slurry in a mortar and pestle, and subsequently cold pressed into a pellet using a hydraulic press upon drying. The pellet was then loaded into an alumina crucible and fired at 1200 °C for 12 h. The sample was allowed to cool to room temperature and was then reground, pressed, and fired at 1500 °C for an additional 12 h. The heating and cooling rates were kept below 5°/min. The final pellet was ground into a fine powder and checked for purity with XRD, which revealed no evidence of impurities.

B. Room temperature neutron diffraction

Structural characterization at 300 K was carried out using neutron diffraction at the Nanoscale-Ordered Materials Diffractometer (NOMAD) beamline [17] at the Spallation Neutron Source at Oak Ridge National Laboratory (ORNL) in Oak Ridge, Tennessee. Despite the large thermal neutron absorption cross section, there is a window of relatively high transmission extending from about 0.25 to 0.7 Å in wavelength, and Dy_2TiO_5 was successfully measured using a small sample size. The sample was first loaded into a 2-mm-diameter quartz capillary filled to a height of 1 cm and measured for a total of 140 min. An identical, empty quartz capillary was also measured for 140 min to serve as a background. Rietveld refinement was performed on diffraction patterns from detector bank 5 with an average scattering angle 2θ of 154° (Q range of 4–49.9 $Å^{-1}$) using the FullProf code [18] to characterize the crystal structure and determine the unit cell parameters and atomic positions within the unit cell. Neutron absorption was accounted for in FullProf through the use of a refinable absorption correction parameter for time-of-flight data with cylindrical geometry.

C. Low temperature XRD and neutron diffraction

The low temperature XRD patterns were measured with a HUBER x-ray powder diffractometer. Unit cell parameters were determined by Rietveld refinement using FullProf. All neutron diffraction measurements at 20 K and below were performed at the Neutron Powder Diffractometer beamline (HB-2A) at the High Flux Isotope Reactor (HFIR) at ORNL. Custom flat-plate holders with a thickness of 0.15 mm were machined from aluminum stock to minimize absorption from Dy atoms. A wavelength of 2.4136 Å was selected using a germanium wafer-stack monochromator to provide higher resolution and access to magnetic Bragg peaks at low scattering angles. Data were collected for 5 h at 0.3 and 20 K and 4 h at intermediate temperatures. Rietveld refinement was performed at 20 K (above the magnetic transition temperature) to determine atomic positions and the unit cell parameters of the crystal structure. The magnetic structure was characterized using representational analysis. The magnetic propagation k vector was determined using the magnetic peaks at 0.3 K with the k-search function in FullProf. Irreducible representations (IRs) and basis vectors were obtained using the SARA*h* representational analysis code [18].

D. Magnetic susceptibility measurements

The dc susceptibility measurements were performed using a Quantum Design superconducting quantum interference device (SQUID) magnetometer. The ac susceptibility was measured at the National High Magnetic Field Laboratory with

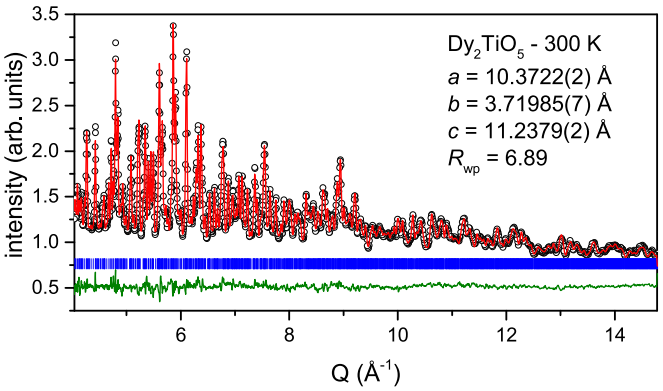

FIG. 2. Room temperature neutron diffraction pattern (open circles) of Dy_2TiO_5 refined with the orthorhombic (*Pnma*) structural model (solid red line). Dy_2TiO_5 can be accurately measured despite dysprosium's large absorption cross section (994 b for thermal neutrons) due to the high flux at the NOMAD beamline. Vertical blue ticks denote Bragg peak positions, while the solid green line is the difference between the measured data and the structural model.

the conventional mutual inductance technique at frequencies between 80 and 700 Hz.

III. RESULTS AND DISCUSSION

A. Structural characterization

1. Neutron diffraction

The previously reported orthorhombic polymorph characteristic of lanthanide titanates of the Ln_2TiO_5 composition agrees well with the measured neutron diffraction data of Dy_2TiO_5 at room temperature (Fig. 2). The unit cell parameters were determined to be $a = 10.3722(2)$ Å, $b = 3.71985(7)$ Å, and $c = 11.2379(2)$ Å. In general, the atom positions agree well with those reported in Ref. [3] which were determined by synchrotron XRD; however, the uncertainty is reduced by nearly an order of magnitude for the oxygen, likely due to the use of neutrons in the present paper (Table I). The mean Dy-O bond length, ⟨Dy-O⟩, differs for each Dy site [2.328(1) Å and 2.345(1) Å, respectively]. Nearest-neighbor Dy atoms (Dy1-Dy2 and Dy2-Dy2) form two-dimensional (2D) "sheets" extending in the [0 1 0] direction [Fig. 3(a)].

There is no evidence of a structural transformation or change of *Pnma* space group down to 0.3 K (although additional diffraction peaks emerge ∼1.75 K due to a magnetic transition, discussed below). The unit cell volume contracts by 0.90(5)%, and ⟨Dy-O⟩ bond lengths are reduced to 2.316(2) and 2.320(2) Å for Dy1 and Dy2, respectively (Table I). Interestingly, Dy2-Dy2 pairs split and are no longer nearest neighbors. Nearest-neighbor Dy atoms (Dy1-Dy2) now form two-atom "ladders" in the [0 1 0] direction [Fig. 3(b)]. The axial positions for the two monocapped octahedra display different temperature dependencies. The O1-Dy2-O3 bond angle becomes increasingly distorted at low temperatures, while the O1-Dy1-O2 is more ridged, with only minor temperature dependence (Fig. 4). At 300 K, both the O1-Dy1-O2 and the O1-Dy2-O3 bond angles are close to 180° [177.4(2)° and 174.6(2)°, respectively]. The bond angle significantly decreases for O1-Dy2-O3 as the temperature is lowered, while it slightly increases for O1-Dy2-O2.

2. XRD measurements

The XRD measurements also show no change in the *Pnma* space group down to 10 K. However, the structure becomes continuously distorted at low temperatures (Fig. 5). This is particularly evident in b, which shows negative thermal expansion below 100 K [Fig. 5(a)]. This has little effect on the unit cell volume as b is only ∼1/3 as large as a and c, which do not show as significant of a distortion [Fig. 5(b)]. It does, however, indicate that the Dy ladders described in Fig. 3(b) become increasingly stretched along [0 1 0] at low temperatures, which could suppress any spin canting in that direction.

B. Magnetic characterization

1. dc susceptibility

Magnetic susceptibility measurements indicate an antiferromagnetic transition with a transition temperature of 3.5 K [Fig. 6(a)]. There is no divergence in zero-field-cooled (ZFC) and field-cooled (FC) measurements below this temperature (not shown), suggesting the absence of any irreversibility. The susceptibility follows the Curie-Weiss law above 3.5 K, indicating paramagnetic behavior. The effective magnetic moment (μ_{eff}) for Dy^{3+} was evaluated to be 10.55 μ_B using the Curie constant C, extracted from the fit to the Curie-Weiss law. This agrees well with the moment for free Dy^{3+} ions, which has a value of 10.63 μ_B. The Curie-Weiss temperature (θ_{CW}) was evaluated to be −10.8 K, suggesting antiferromagnetic interactions. Magnetization measurements as a function of increasing field show saturation far below the effective moment for each Dy^{3+} [Fig. 6(b)]. This is indicative of strong anisotropy for Dy^{3+} spins, similar to that observed for the cubic $Dy_2(Ti_{2-x}Dy_x)O_{7-x/2}$ and $Ho_2(Ti_{2-x}Ho_x)O_{7-x/2}$ polymorphs [10,19–21]. Interestingly, magnetization measurements in these previous papers saturate at half (or slightly below) the moment for free Dy^{3+} or Ho^{3+}. The orthorhombic polymorph in the present paper, however, saturates closer to 65% of the moment for free Dy^{3+}, suggesting that anisotropy is partially relieved relative to spin ice in pyrochlore.

2. ac susceptibility

Zero-field ac magnetic susceptibility measurements also show evidence of a paramagnetic to antiferromagnetic transition beginning at 3.1 K, as noted by the sluggish downturn in the real part of magnetic susceptibility, χ' [Fig. 7(a)]. There exists only weak frequency dependence, suggesting the absence of glass/ice-like dynamics. The magnetic structure is, however, strongly field dependent. There are two peaks in the field scan performed at 0.3 K [Fig. 7(b)]. Each of the moments on both Dy^{3+} atoms (Dy1 and Dy2, discussed earlier) are likely polarized by the magnetic field independently as the magnitude of the two peaks in the field scan is identical. Cooling in the presence of a 1 T magnetic field slightly sharpens the transition and lowers the maximum to 1.1 K [Fig. 7(c)]. A 2 T magnetic field suppresses susceptibility and further lowers the maximum to 0.8 K. Larger fields completely dampen the magnetic transition. There is a small kink at 1.6 K, which is

TABLE I. Refined structural parameters for orthorhombic Dy_2TiO_5 at 300 K and 0.3 K determined by neutron diffraction. Data at 300 K was collected at the NOMAD beamline of the Spallation Neutron Source while data at 0.3 K was collected at the Hb-2a beamline of the High Flux Isotope Reactor. The displacement parameter, U_{iso}, was fixed for measurements at 0.3 K. Dy2 and Ti are not coordinated with O4 and O1 respectively (indicated by dashes).

300 K	a (Å)	b (Å)	c (Å)	V(Å^3)		
Pnma	10.3722(2)	3.71985(7)	11.2379(2)	433.59(1)		
Atom	x	y	z	U_{iso}		
Dy1	0.11421(13)	0.25	0.22290(11)	0.0056(3)		
Dy2	0.13611(13)	0.25	0.55759(13)	0.0062(3)		
Ti1	0.1740(6)	0.25	0.8833(7)	0.0081(9)		
O1	0.4948(4)	0.25	0.1032(4)	0.0070(6)		
O2	0.2255(4)	0.25	0.0433(4)	0.0098(8)		
O3	0.2598(4)	0.25	0.7294(4)	0.0069(7)		
O4	0.5097(5)	0.25	0.6537(4)	0.0146(10)		
O5	0.2659(4)	0.25	0.3833(4)	0.0065(7)		
Bond length (Å)	O1	O2	O3	O4	O5	⟨X-O⟩
Dy1	2.314(5)	2.325(5)	2.227(3)×2	2.391(3)×2	2.393(5)	2.328(1)
Dy2	2.327(5) 2.359(3)×2	2.355(3) × 2	2.318(5)	–	2.377(5)	2.350(2)
Ti	–	1.876(9)	1.945(9)	1.754(8)	1.962(2)×2	1.900(3)
0.3 K	a (Å)	b (Å)	c (Å)	V(Å^3)		
Pnma	10.344(2)	3.7114(8)	11.193(2)	429.74(16)		
Atom	x	y	z	U_{iso}		
Dy1	0.116(2)	0.25	0.225(1)	0.0038		
Dy2	0.143(2)	0.25	0.559(1)	0.0038		
Ti1	0.216(7)	0.25	0.854(11)	0.0038		
O1	0.500(6)	0.25	0.091(6)	0.0038		
O2	0.244(5)	0.25	0.035(6)	0.0038		
O3	0.249(7)	0.25	0.741(4)	0.0038		
O4	0.485(4)	0.25	0.662(4)	0.0038		
O5	0.261(6)	0.25	0.368(5)	0.0038		
Bond length (Å)	O1	O2	O3	O4	O5	⟨X-O⟩
Dy1	2.38(7)	2.50(7)	2.33(5)×2	2.24(3)×2	2.19(7)	2.316(2)
Dy2	2.24(7) 2.40(5)×2	2.21(4)×2	2.31(6)	–	2.47(6)	2.320(2)
Ti	–	2.06(14)	1.31(13)	2.40(10)	1.877(18)×2	1.90(4)

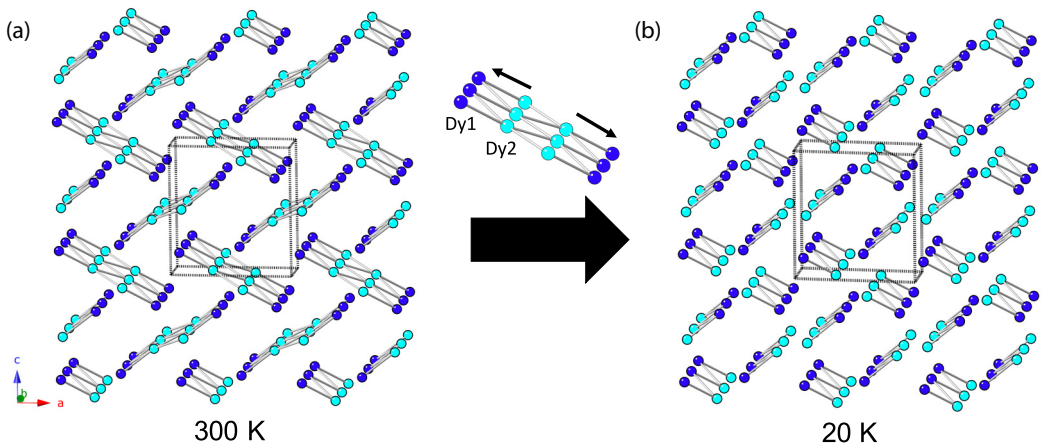

FIG. 3. Dy sublattice of Dy_2TiO_5. (a) Dy1 (dark blue spheres) has two Dy2 (cyan spheres) nearest neighbors at 300 K, while Dy2 is a neighbor with two Dy2 atoms. (b) At 20 K, Dy2-Dy2 pairs are split and are no longer nearest neighbors. Dy1 is a nearest neighbor with two Dy2 atoms, while Dy2 is a nearest neighbor with Dy1 atoms.

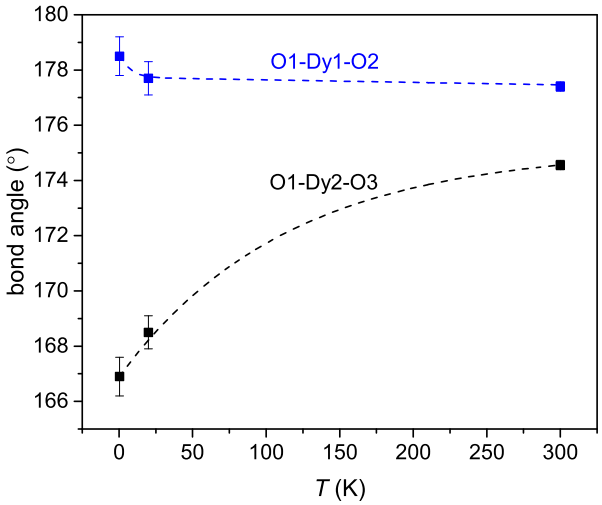

FIG. 4. Axial bond angle temperature dependence for Dy1 and Dy2 monocapped octahedra determined by neutron diffraction. O1-Dy1-O2 becomes more symmetrical at lower temperatures, while O1-Dy2-O3 becomes more distorted. The dashed lines are guides to the eye. Refer to Fig. 12 for a detailed explanation of these oxygen positions.

first apparent in the 2 T measurement. This is an artifact due to He^3 condensation as the position is invariant at stronger magnetic fields.

A peak in susceptibility is commonly assigned to the onset of long-range order. However, the downturn is broader than expected for a transition to long-range magnetic order. There is also an observable inflection in χ' below the maximum at 3.1 K for the zero-field measurements of Dy_2TiO_5 in Figs. 7(a) and 7(c). This is most apparent when looking at $d\chi'/dT$ as sharp peaks are evident at 1.7 and 0.6 K for 0 and 1 T measurements, respectively [Fig. 7(d)]. The rapid increase in $d\chi'/dT$ that occurs ~3 K corresponds to the maximum observed in χ''. It has been previously argued that the onset of long-range antiferromagnetic ordering can be better predicted by a peak in the first derivative of χ' [22], suggesting that long-range ordering may not begin until 1.7 K. This possibly implies that short-range ordering at 3.1 K precedes the onset of long-range ordering at 1.7 K. However, because the ac susceptibility shows little to no frequency dependence, this could also indicate a shift in the dimensionality of magnetic order, that is, a 2D to three-dimensional (3D) transition, with $T_{N,2D} = 3.1$ K and $T_{N,3D} = 1.7$ K. Low temperature neutron diffraction provides more insight into the dimensionality of the spin structure.

3. Magnetic neutron diffraction

A magnetic transition is confirmed with neutron diffraction experiments [Fig. 8(a)]. Comparing the background of the diffraction patterns taken at 20 and 3 K reveals the onset of local magnetic ordering, as noted by the appearance of a broad, diffuse peak centered at $2\theta \approx 22.5°$. Strong resolution limited Bragg peaks are apparent at 0.3 K. These peaks can be indexed with a propagation vector $k = [0\ 1/2\ 0]$. The diffuse peak at 3 K and the (100) magnetic peak at 0.3 K are centered at the same scattering angle but with a different peak shape [Fig. 8(b)]. To test the lower dimensionality suggested by susceptibility measurements, the diffuse peak was fitted with a Warren function characteristic of 2D magnetic ordering [23–26]:

$$P(\theta) = Kmf_{hk}^2 \frac{(1+\cos^2 2\theta)}{2(\sin\theta)^{\frac{3}{2}}} \left(\frac{\xi}{\lambda\sqrt{\pi}}\right)^{\frac{1}{2}} F(a) \qquad (1)$$

where

$$F(a) = \int_0^{20} \exp[-(x^2 - a)^2]dx \qquad (2)$$

and

$$a = \frac{2\xi\sqrt{\pi}}{\lambda}(\sin\theta - \sin\theta_0) \qquad (3)$$

in which K represents a scale factor, m represents the multiplicity of the reflection, F_{hk}^2 represents the magnetic structure factor, ξ represents the spin-spin correlation length,

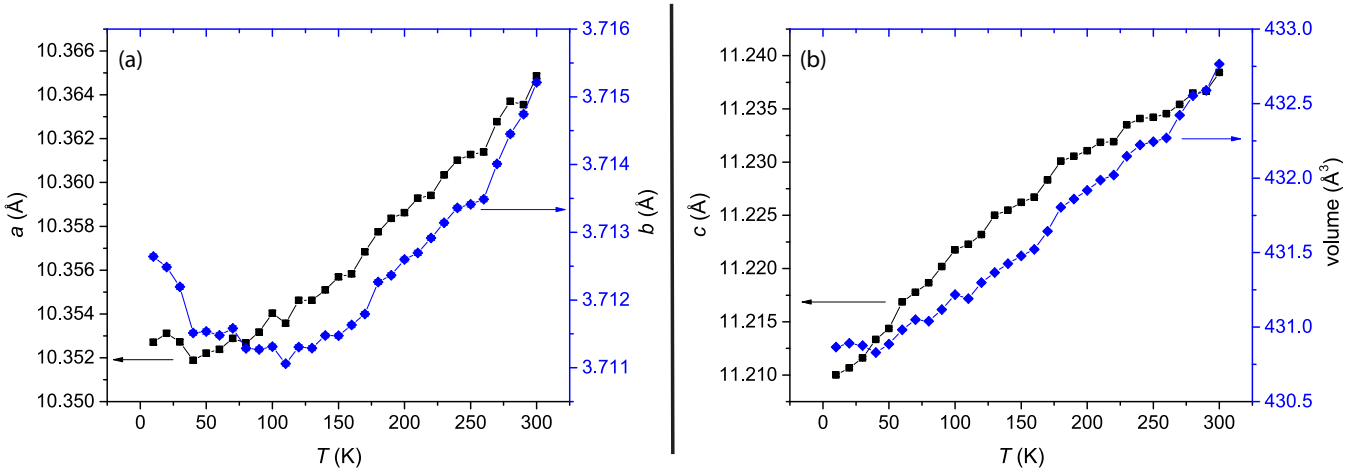

FIG. 5. Low temperature XRD patterns. (a) The a unit cell parameter (black squares, left axis) indicates only a slight distortion at low temperatures, while b (blue diamonds, right axis) shows a continual increase below 100 K. (b) Unlike a and b, the c unit cell parameter (black squares, left axis) continually decreases with temperature. The contraction of the unit cell volume (blue diamonds, right axis) saturates below 40 K.

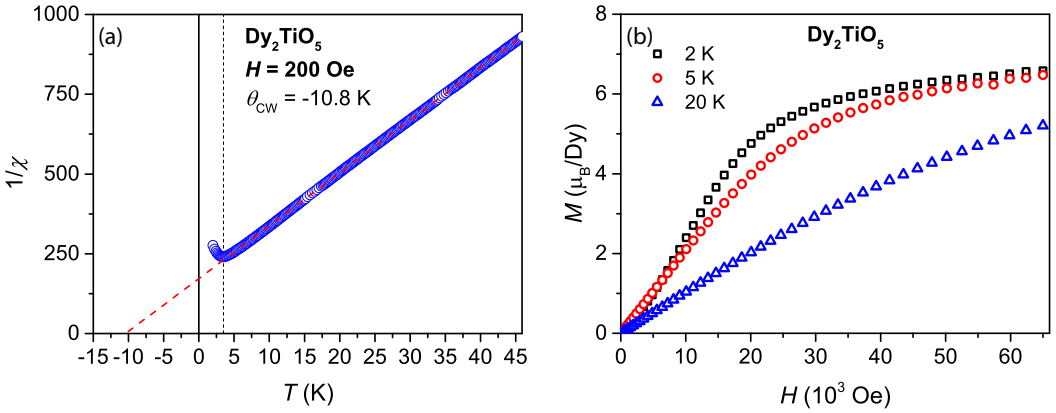

FIG. 6. The dc magnetic susceptibility and magnetization measurements of Dy_2TiO_5. (a) Inverse susceptibility reveals an antiferromagnetic transition at 3.5 K (vertical dashed line) with paramagnetic behavior above this temperature. The Curie-Weiss law was fit to the data (dashed red line), resulting in a Curie-Weiss temperature (θ_{CW}) of −10.8 K. (b) Magnetization measurements at varying temperatures show saturation below the moment for free Dy^{3+} ions but larger than that observed in spin-ice or cubic Dy_2TiO_5 polymorphs.

and θ_0 represents the centroid of the diffuse peak. The integral in $F(a)$ was evaluated numerically and agrees with values reported in Ref. [23]. The Warren function fits the diffuse peak well with $\xi \approx 22$ Å (Fig. 9). This agrees with the susceptibility measurements and is strongly suggestive of low dimensionality ordering. A simple linear background was included in the fitting procedure, consistent with Ref. [26].

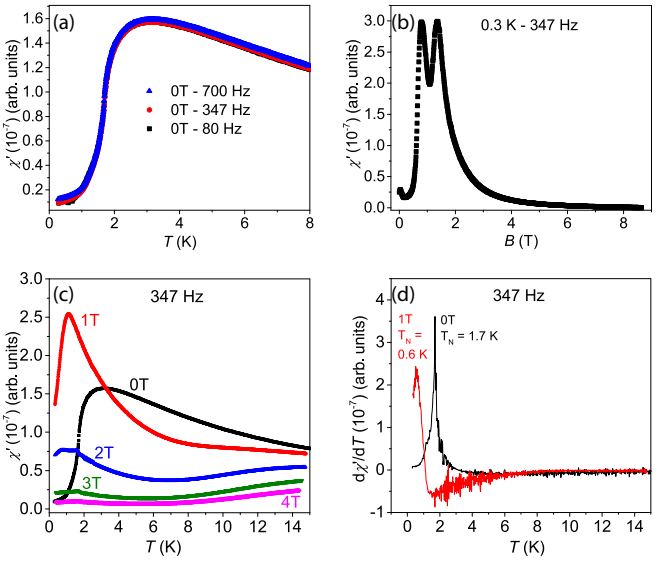

FIG. 7. The ac magnetic susceptibility measurements of powder Dy_2TiO_5. (a) Real part of zero-field ac magnetic susceptibility at 700, 347, and 80 Hz. There is only weak frequency dependence, suggesting the absence of local ice/glassy dynamics. A sluggish paramagnetic to antiferromagnetic transition is apparent at 3.1 K. (b) Magnetic field sweep at 0.3 K with a frequency of 347 Hz. There are two maxima of equal intensity at 0.79 and 1.35 T. (c) Real part of magnetic susceptibility of B = 0–4 T. The magnetic field initially decreases the ordering temperature and sharpens the magnetic transition. The transition temperatures are 3.1, 1.1, and 0.8 K for 0, 1, and 2 T, respectively. Stronger fields completely dampen the transition. (d) First derivative of the real part of magnetic susceptibility for B = 0 and 1 T. Sharp peaks are apparent at 1.7 and 0.6 K for 0 and 1 T, which correspond to the onset of long-range magnetic order.

Although local ordering begins at 3 K, a long-range magnetic transition (T_N) is not apparent until 1.7 K, as noted by the temperature dependence of the (100) magnetic peak intensity [Fig. 8(b), inset], explaining the sluggish transition observed in susceptibility [Fig. 7(a)] and the sharp maximum observed in the first derivative curve [Fig. 7(d)]. This also suggests that Dy_2TiO_5 is only moderately frustrated, as the frustration parameter f (defined as $|\theta_{CW}|/T_N$) is equal to 6.4.

Each Dy atom occupies a 4*c* Wyckoff site within the *Pnma* symmetry, creating four equivalent positions for each Dy atom (translations are shown below):

$$\begin{aligned}
&\text{atom 1}: x, y, z\\
&\text{atom 2}: x+\tfrac{1}{2}, -y+\tfrac{1}{2}, -z+\tfrac{1}{2}\\
&\text{atom 3}: -x+1, y+\tfrac{1}{2}, -z+\tfrac{1}{2}\\
&\text{atom 4}: -x+\tfrac{1}{2}, -y+1, z+\tfrac{1}{2}
\end{aligned}$$

There exist two equivalent IRs, each with 12 basis vectors (ψ_n). One IR was ultimately chosen for magnetic characterization. The magnetic state is therefore described by a linear combination of 12 basis vectors (6 basis vectors each for Dy1 and Dy2, shown in Table II). The coefficients on ψ_1 must have opposite signs for Dy1 and Dy2; otherwise, there are prominent forbidden reflections at $2\theta = 18.7, 33.1, 42.5$, and 54.9, among other minor reflections. This also applies to the coefficients for ψ_4. Conversely, the coefficients on ψ_2 for Dy1 and Dy2 must have the same sign to eliminate forbidden reflections at $2\theta = 52.5$ and 66.2. An analogous relationship holds for ψ_5. The coefficients on ψ_3 must be of opposite signs for Dy1 and

TABLE II. Symmetrically allowed basis vectors (BVs) for the Γ_2 IR for the *Pnma* space group with a $k = [0\ 1/2\ 0]$ propagation vector. Dy1 and Dy2 do not need to have the same combination of BVs.

	Atom 1			Atom 2				Atom 3			Atom 4		
BV	m_x	m_y	m_z	m_x	m_y	m_z	BV	m_x	m_y	m_z	m_x	m_y	m_z
ψ_1	2	0	0	2	0	0	ψ_3	0	$\bar{2}$	0	0	$\bar{2}$	0
ψ_2	0	0	2	0	0	$\bar{2}$	ψ_4	$\bar{2}$	0	0	$\bar{2}$	0	0
ψ_6	0	2	0	0	2	0	ψ_5	0	0	$\bar{2}$	0	0	2

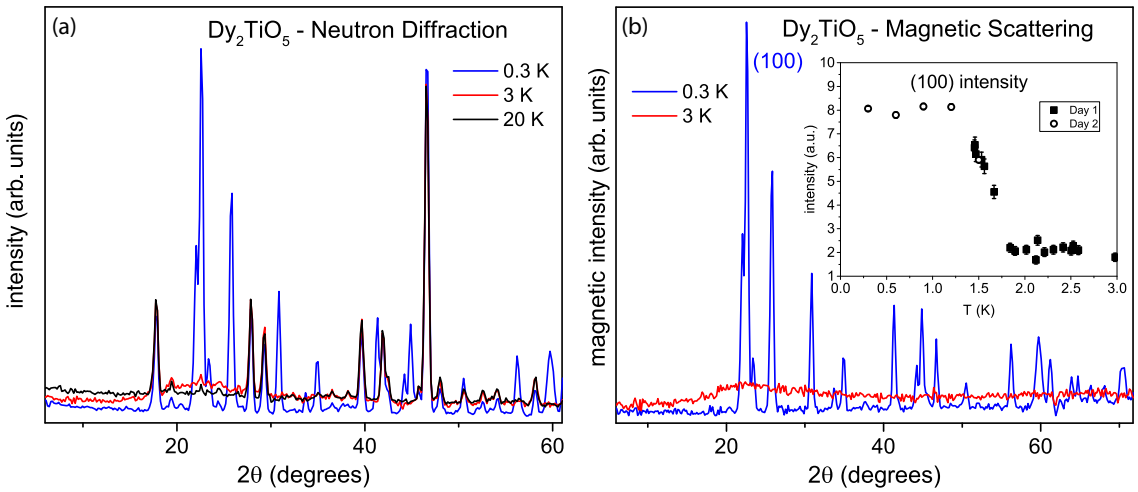

FIG. 8. Low temperature neutron scattering patterns. (a) Neutron diffraction patterns at 0.3, 3, and 20 K. (b) Magnetic contributions only at 0.3 and 3 K obtained by subtracting the pattern at 20 K. Only diffuse magnetic scattering is observed at 3 K, while long-range magnetic order begins ∼1.7 K (inset). Solid squares and open circles were measured on separate days.

Dy2 to remove forbidden reflection at $2\theta = 33.1$, 42.5, and 52.5, among others, which also applies to ψ_6. There remain, however, low intensity forbidden reflections, indicating that any moment canting in the [0 1 0] direction is unlikely and this component was fixed at zero. This agrees with the negative thermal expansion observed in Fig. 5(a), in which Dy atoms become increasingly separating along b at low temperatures. Assuming that C_n is equal for both Dy1 and Dy2 atoms, despite them occupying crystallographically independent sites, produces a reasonable fit to the experimental data ($R_{WP} = 18.3$; Table III). The calculated moment is 8.05(12) μ_B, which is reasonable but still less than the ordered moment of 10 μ_B for free Dy^{3+} ions, suggesting that moments are not fully saturated, even at 0.3 K, or are dampened by crystal field effects. The fit is significantly improved by removing the constraint that moments be equal for Dy1 and Dy2 atoms ($R_{WP} = 13.8$; Fig. 10). This results in a magnetic moment of 8.89(28) μ_B and 7.76(31) μ_B for Dy1 and Dy2, respectively (Table III). The spin directions within the magnetic structure in both scenarios follow the underlying interwoven 2D sheets created by the Dy ions (Fig. 11). This ordering could explain the 2D-3D magnetic transition suggested earlier. One possible mechanism is that moments order on 2D ladders created by nearest-neighbor Dy1-Dy2 pairs at 3 K [Fig. 3(b) and gray lines in Fig. 11] but do not interact with other pairs on longer scales. Beginning at 1.7 K, locally ordered moments on these ladders interact with neighboring Dy1-Dy2 pairs, forming the interwoven structure shown in Fig. 11. It should be noted that there is an additional magnetic peak at $2\theta = 23.9°$ that cannot be indexed with the $k = [0\ 1/2\ 0]$ propagation vector and either requires a larger unit cell, is suggestive of an incommensurate magnetic structure, or is due to an unidentified low temperature phase within the measured sample.

The refined Dy1 moments always point along the O1-Dy1-O2 bond angle (Fig. 12), which is nearly 180° [178.5(7)°]. This is indicative of a local Ising axis, explaining the anisotropy observed in the magnetization measurements discussed earlier.

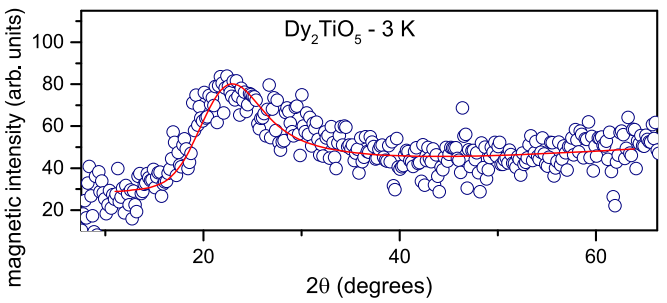

FIG. 9. Fit of the diffuse magnetic scattering at 3 K using the Warren function.

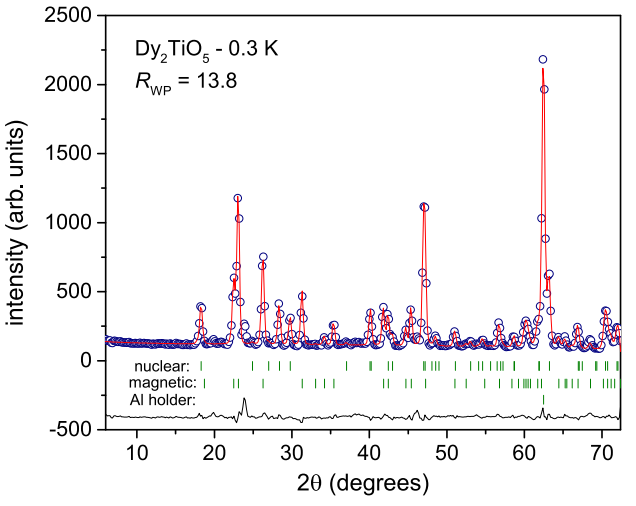

FIG. 10. Magnetic neutron refinement at 0.3 K. The refinement (solid red line) agrees well with the measured data (open circles). The nuclear structure, magnetic structure, and Al holder were all refined together. Refined Bragg peaks from each phase are shown as vertical green ticks. The solid black line represents the difference between measured data and refinement. There exists an additional magnetic peak at 23.8° that cannot be indexed with the $k = [0\ 1/2\ 0]$ propagation vector and requires a larger unit cell.

TABLE III. Refined coefficients for magnetic basis vectors. C_n refers to the coefficient on ψ_n described in Table II. Data were collected at 0.3 K at the HB-2A beamline of the HFIR. The refinement is improved if coefficients on Dy1 and Dy2 are independently refined.

				Same moments ($R_{WP} = 18.3$)			
Atom	C_1	C_2	C_3	C_4	C_5	C_6	μ
Dy1	2.61(6)	− 3.06(6)	0	− 2.61(6)	3.06(6)	0	8.05(12)
Dy2	− 2.61(6)	− 3.06(6)	0	2.61(6)	3.06(6)	0	8.05(12)
				Different moments ($R_{WP} = 13.9$)			
Atom	C_1	C_2	C_3	C_4	C_5	C_6	μ
Dy1	2.35(15)	− 3.78(13)	0	− 2.35(15)	3.78(13)	0	8.89(28)
Dy2	− 3.00(17)	− 2.46(12)	0	3.00(17)	2.46(12)	0	7.76(31)

However, Dy2 does not possess such an "easy axis." O1, O3, and O5 all reside within a (0 1 0) plane; however, none make a 180° bond angle with Dy2. The O1-Dy2-O3 bond angle is 167.2(7)°, while O5 is an octahedral monocap without an equivalent oxygen in line with Dy2. The Dy2 moments order nearly along the O1-Dy2-O3 bond angle but are canted slightly toward O5.

The angle between O4-Dy2-O5 is close to 180° [177.9(6)°] and nearly parallel to O1-Dy1-O2, which could provide a local Ising axis; however, the Dy2-O4 spacing [3.5243(6) Å] is far beyond the ionic radius of Dy^{3+}. This axis would also be forbidden by the restrictions set on the basis vectors earlier as Dy1 and Dy2 must have opposite signs for ψ_1 and same signs for ψ_2. These cannot be simultaneously fulfilled for this direction. Thus, Dy2 moments do not order in a particular direction with strong uniaxial symmetry, as required for Ising-like ordering.

This is consistent with the observed dc magnetization measurements. The anisotropic Dy1 spins lower the magnetization saturation point, much like Dy spins in $Dy_2Ti_2O_7$ spin ice (approximately ½ of the free Dy^{3+} moment). The more isotropic Dy2 spins, however, raise the saturation relative to spin-ice pyrochlores (and cubic A_2TiO_5 polymorphs), resulting in bulk saturation that is between spin-ice and free Dy^{3+}. The distinct ordering and anisotropies for Dy1 and Dy2 potentially explain the double peak in the magnetic field scan at 0.3 K [Fig. 7(b)]. In general, a sharp peak is indicative of a spin-flip transition. The double peak therefore indicates two successive spin-flip transitions. Since there are two unique Dy ions, the most likely cause of this is that one peak corresponds to Dy1 and the other corresponds to Dy2. The difference in the applied fields for the peaks therefore reflects the different energy scales of the magnetic exchange interactions for Dy1 and Dy2. The origins of this in the lattice, as discussed, are the different crystal field and bond angles that lead to more Ising-like interactions for one Dy and less for the other. To assign the observed peaks, in general, Ising transitions are typically sharper than non-Ising (Heisenberg) transitions. The

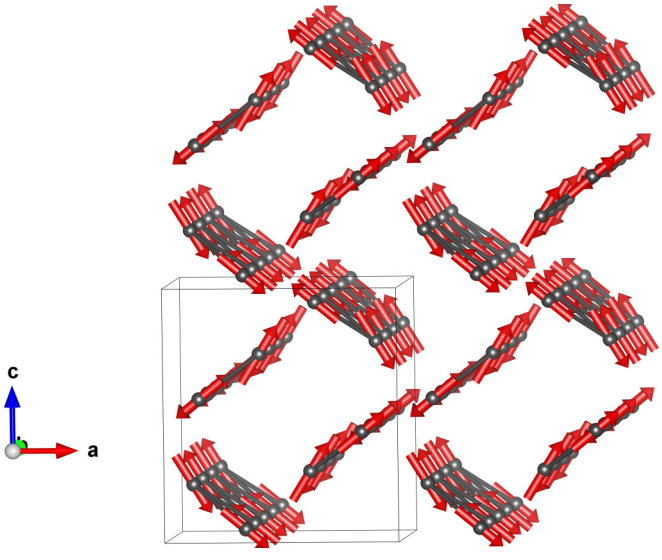

FIG. 11. Refined magnetic structure of Dy_2TiO_5. Dy atoms are shown as gray spheres, while magnetic moments are shown as red arrows. Solid gray lines designate nearest-neighbor Dy pairs. Ordered moments encircle nonmagnetic Ti^{4+} cations (not shown).

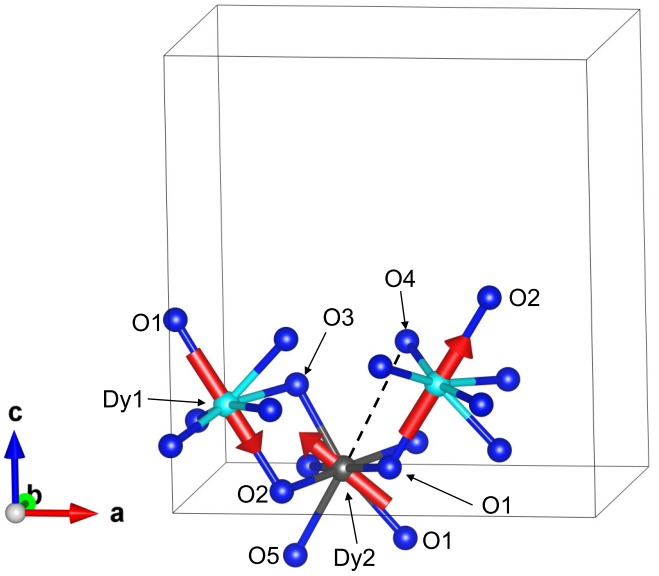

FIG. 12. Relation between refined magnetic moments and oxygen coordination for Dy1 and Dy2 at 0.3 K. Magnetic moments on Dy1 atoms (cyan spheres) order along the 180° angle formed by O1-Dy1-O2, which corresponds to a local Ising axis. Dy2 (black sphere) does not possess such a crystal field, and the moment is ordered between O1-Dy2-O3 and O1-Dy2-O5 bond angles. O5-Dy2-O4 forms a 180° angle that is nearly parallel to O1-Dy1-O2; however, the Dy2-O4 distance (shown as a dashed line) is far beyond the ionic radius of Dy^{3+}.

first peak in Fig. 7(b) at 0.79 T, which is slightly narrower than the second peak at 1.35 T, could therefore correspond to Ising-like Dy1 spin flips. This assignment is further supported by examining the number of next-nearest neighbors available for exchange interactions. As shown in Figs. 3 and 11, Dy atoms are ordered in sheets extending infinitely in the [010] direction. Dy1 atoms form the edges of the sheet, while Dy2 atoms are on the interior (Dy1-Dy2-Dy2-Dy1). Dy2 has four next-nearest neighbors that are approximately equidistant: two in the [010] direction and two that were originally nearest neighbors at 300 K [Fig. 3(a)]. Dy1 atoms, however, only have the two next-nearest neighbors in the [010] direction because they are not interior atoms. If Dy2 moments were to flip first (at 0.79 T), Dy1 spins would be isolated and rely solely on Dy1-Dy1 coupling in the [010] direction to remain ordered. If Dy1 atoms flipped first, however, Dy2 could still maintain order (with itself) within the sheet. Unless the Dy1-Dy1 coupling strength is very strong, the peaks at 0.79 and 1.35 T can be reasonably attributed to flipping/polarizing Dy1 and Dy2 spins, respectively. However, this is a complex problem, and without the availability of a single crystal, there are not sufficient data to definitively determine the origin of the double peak since there are many interactions involved (i.e., nearest-neighbor and next-nearest-neighbor exchange, spin anisotropy, and long-range dipolar interactions).

IV. CONCLUSIONS

The structure and magnetic properties of orthorhombic Dy_2TiO_5 have been successfully determined using neutron diffraction, magnetic susceptibility, and magnetization from 300 to 0.3 K. The ac susceptibility shows evidence of a 2D-3D magnetic transition, as noted by the sluggish antiferromagnetic transition beginning at 3 K and inflection at 1.7 K. Neutron diffraction shows that local magnetic ordering (beginning at 3 K) precedes long-range magnetic ordering (beginning at 1.7 K), explaining the ac susceptibility behavior. Magnetic ordering saturates at 1.2 K; however, refined magnetic moments are slightly less than the ordered moment for both Dy1 and Dy2 [$8.89(28)\,\mu_B$ and $7.76(31)\,\mu_B$, respectively]. The magnetic structure can be indexed with a propagation vector of $k = [0\,1/2\,0]$. Moments order in interwoven 2D sheets extending in the [0 1 0] direction, which encircle nonmagnetic Ti atoms. Dy1 shows Ising-like ordering along local O1-Dy1-O2 axes, while Dy2 does not possess a direction of uniaxial symmetry.

ACKNOWLEDGMENTS

J.S. acknowledges support from Organized Research Unit funding through the University of Tennessee Office of Research. Z.L.D. and H.D.Z. acknowledge support from the National Science Foundation (NSF) Contract No. NSF-DMR-1350002. A portion of this research used resources at the High Flux Isotope Reactor and Spallation Neutron Source, a DOE Office of Science User Facility operated by the Oak Ridge National Laboratory. A portion of this work was performed at the National High Magnetic Field Laboratory, which is supported by NSF Cooperative Agreement No. DMR-1157490 and the State of Florida. M.L.'s effort and the sample preparation were supported as a part of the Material's Science of Actinides, an Energy Frontier Research Center funded by the US Department of Energy, Office of Science, Basic Energy Sciences under Award No. DE-SC0001089.

[1] W. G. Mumme and A. D. Wadsley, Acta Crystallogr. B Struct. Crystallogr. Cryst. Chem. **24**, 1327 (1968).
[2] A. V. Shlyakhtina, D. A. Belov, O. K. Karyagina, and L. G. Shcherbakova, J. Alloy. Comp. **479**, 6 (2009).
[3] R. D. Aughterson, G. R. Lumpkin, G. J. Thorogood, Z. M. Zhang, B. Gault, and J. M. Cairney, J. Solid State Chem. **227**, 60 (2015).
[4] Y. F. Shepelev and M. A. Petrova, Inorg. Mater. **44**, 1354 (2008).
[5] M. A. Petrova and R. G. Grebenshchikov, Glass Phys. Chem. **34**, 603 (2008).
[6] K. E. Sickafus, L. Minervini, R. W. Grimes, J. A. Valdez, M. Ishimaru, F. Li, K. J. McClellan, and T. Hartmann, Science **289**, 748 (2000).
[7] R. C. Ewing, W. J. Weber, and J. Lian, J. Appl. Phys. **95**, 5949 (2004).
[8] W. J. Weber, R. C. Ewing, C. R. A. Catlow, T. D. de la Rubia, L. W. Hobbs, C. Kinoshita, H. Matzke, A. T. Motta, M. Nastasi, E. K. H. Salje, E. R. Vance, and S. J. Zinkle, J. Mater. Res. **13**, 1434 (1998).
[9] Y. Jiang, J. R. Smith, and G. R. Odette, Acta Mater. **58**, 1536 (2010).
[10] G. C. Lau, B. D. Muegge, T. M. McQueen, E. L. Duncan, and R. J. Cava, J. Solid State Chem. **179**, 3126 (2006).
[11] M. J. Harris, S. T. Bramwell, D. F. McMorrow, T. Zeiske, and K. W. Godfrey, Phys. Rev. Lett. **79**, 2554 (1997).
[12] S. T. Bramwell and M. J. P. Gingras, Science **294**, 1495 (2001).
[13] G. C. Lau, R. S. Freitas, B. G. Ueland, B. D. Muegge, E. L. Duncan, P. Schiffer, and R. J. Cava, Nat. Phys. **2**, 249 (2006).
[14] A. P. Ramirez, A. Hayashi, R. J. Cava, R. Siddharthan, and B. S. Shastry, Nature **399**, 333 (1999).
[15] V. D. Risovany, E. E. Varlashova, and D. N. Suslov, J. Nucl. Mater. **281**, 84 (2000).
[16] A. Sinha and B. P. Sharma, J. Am. Ceram. Soc. **88**, 1064 (2005).
[17] J. Neuefeind, M. Feygenson, J. Carruth, R. Hoffmann, and K. K. Chipley, Nucl. Instrum. Meth. Physica Res. B **287**, 68 (2012).
[18] A. S. Wills, Physica B **276–278**, 680 (2000).
[19] D. J. P. Morris, D. A. Tennant, S. A. Grigera, B. Klemke, C. Castelnovo, R. Moessner, C. Czternasty, M. Meissner, K. C. Rule, J. U. Hoffmann, K. Kiefer, S. Gerischer, D. Slobinsky, and R. S. Perry, Science **326**, 411 (2009).
[20] B. G. Ueland, G. C. Lau, R. S. Freitas, J. Snyder, M. L. Dahlberg, B. D. Muegge, E. L. Duncan, R. J. Cava, and P. Schiffer, Phys. Rev. B **77**, 144412 (2008).

[21] G. C. Lau, R. S. Freitas, B. G. Ueland, M. L. Dahlberg, Q. Huang, H. W. Zandbergen, P. Schiffer, and R. J. Cava, Phys. Rev. B **76**, 054430 (2007).
[22] M. E. Fisher, Phil. Mag. **7**, 1731 (1962).
[23] B. E. Warren, Phys. Rev. **59**, 693 (1941).
[24] J. E. Greedan, J. Mater. Chem. **11**, 37 (2001).
[25] A. S. Wills, N. P. Raju, C. Morin, and J. E. Greedan, Chem. Mater. **11**, 1936 (1999).
[26] C. S. Knee, D. J. Price, M. R. Lees, and M. T. Weller, Phys. Rev. B **68**, 174407 (2003).